POLISH POLAR RESEARCH	22	2	129–146	2001

Piotr ŚRODA

Instytut Geofizyki
Polska Akademia Nauk
Ks. Janusza 64, 01-452 Warszawa, POLAND
e-mail: psroda@igf.edu.pl

Three-dimensional modelling of the crustal structure in the contact zone between Antarctic Peninsula and South Pacific from seismic data

ABSTRACT: During four Polish Geodynamical Expeditions to West Antarctica between 1979 and 1991, seismic measurements were made along 21 deep refraction profiles in the Bransfield Strait and along the coastal area of Antarctic Peninsula using explosion sources. Recordings were made by 16 land stations and 8 ocean bottom seismometers. Good quality recordings were obtained up to about 250 km distance. This allowed a detailed study of the seismic wave field and crustal structure. Three-dimensional tomographic inversion was carried out using first arrivals from the complete data set including off-line recordings. As a result, we obtained a 3-D model of the P-wave velocity distribution in the study area. In the area adjacent to the Antarctic Peninsula coast, sedimentary cover of 0.2 to 3 km thickness was found, whereas in the shelf area and in the Bransfield Strait sedimentary basins with thickness from 5 to 8 km were observed. In the Bransfield Strait a high velocity body with $Vp > 7.5$ km/s was found at 12 km depth. The use of the off-line data allowed for determination of the horizontal extent of the body. The thickness of the crust varies from more than 35–40 km in the coastal area south of the Hero Fracture Zone to 30–35 km in the area of Bransfield Strait and South Shetland Islands and about 12 km in the Pacific Ocean NW of South Shetland Islands.

Key words: Antarctic Peninsula, seismic modelling, tomography, crustal structure.

Introduction

The seismic data analyzed in this work were collected during four Polish Geodynamical Expeditions to West Antarctica organized by the Institute of Geophysics of the Polish Academy of Sciences over a span of 11 years starting in 1979/1980. The main purpose was to investigate the deep structure and physical properties of the Earth's crust in the area between Adelaide Island and Elephant Is-

land (Fig. 1), especially in the tectonically active zones and contact zones between lithospheric plates.

The seismic experiments yielded a rich and unique data set containing information about the structure of the Antarctic Peninsula area. A tomographic inversion method was applied to the data in order to create a 3-D model of the Vp velocity distribution in the Earth's crust in the approximately 1000 km long and 300 km wide area along the western coast of the Antarctic Peninsula. The results of the tomographic modelling are described in this paper.

During the refraction and wide-angle reflection studies, seismic waves were generated by underwater explosions of TNT charges ranging from 16 to 144 kg in size, usually 50–100 kg, at depth of 60 m. The distance between shot locations was about 6 km. About 510 shots were detonated. Seismic waves were recorded on land by portable seismic recorders. All expeditions used a total of 16 land locations. During the last expedition, land stations were supplemented with 9 Ocean Bottom Seismometers (OBS), provided by the Hokkaido University.

Geology of the study area

The Antarctic Peninsula, a part of West Antarctica, is a 1500 km long strip of the continental crust separating the southeast Pacific Ocean from the Weddell Sea (Fig. 1). According to Garrett and Storey (1987), West Antarctica was a place of continuous subduction of Pacific and proto-Pacific lithosphere from at least the early Mesozoic until the late Tertiary. At the beginning of the Gondwana breakup, about 170 Ma ago (Early Jurassic), the Antarctic Peninsula partially began to separate from the Antarctic continent due to spreading which created the Weddell Sea (Lawver *et al.* 1991), a back-arc basin filled by thick clastic sediments. This extensional episode lasted until the earliest Cretaceous. The arc and back-arc were subject to heavy deformation during the Early to Middle Cretaceous compressional episode (Meneilly *et al.* 1987). During the Late Cretaceous–Tertiary, the intra-arc extension occurred. The extension has been probably caused by slowing and finally stopping of subduction due to ridge crest-trench collisions (Garrett and Storey 1987).

Subduction of the Pacific seafloor has ceased progressively from SW to NE following ridge crest-trench collisions. The first collision probably occurred in the south of the Antarctic Peninsula at about 50 Ma (Henriet *et al.* 1992). When subduction and spreading in a given segment stopped, the corresponding part of the subduction zone became a passive continental margin. The magmatism ceased and the segment was uplifted and eroded. The last collision took place in the segment south of the Hero Fracture Zone during the Pliocene, 6.5 to 4 Ma ago (Barker 1982). Subducted fracture zones are reflected in the overlying crust of the Antarctic Peninsula as the transverse megafractures, dividing it into regions with different

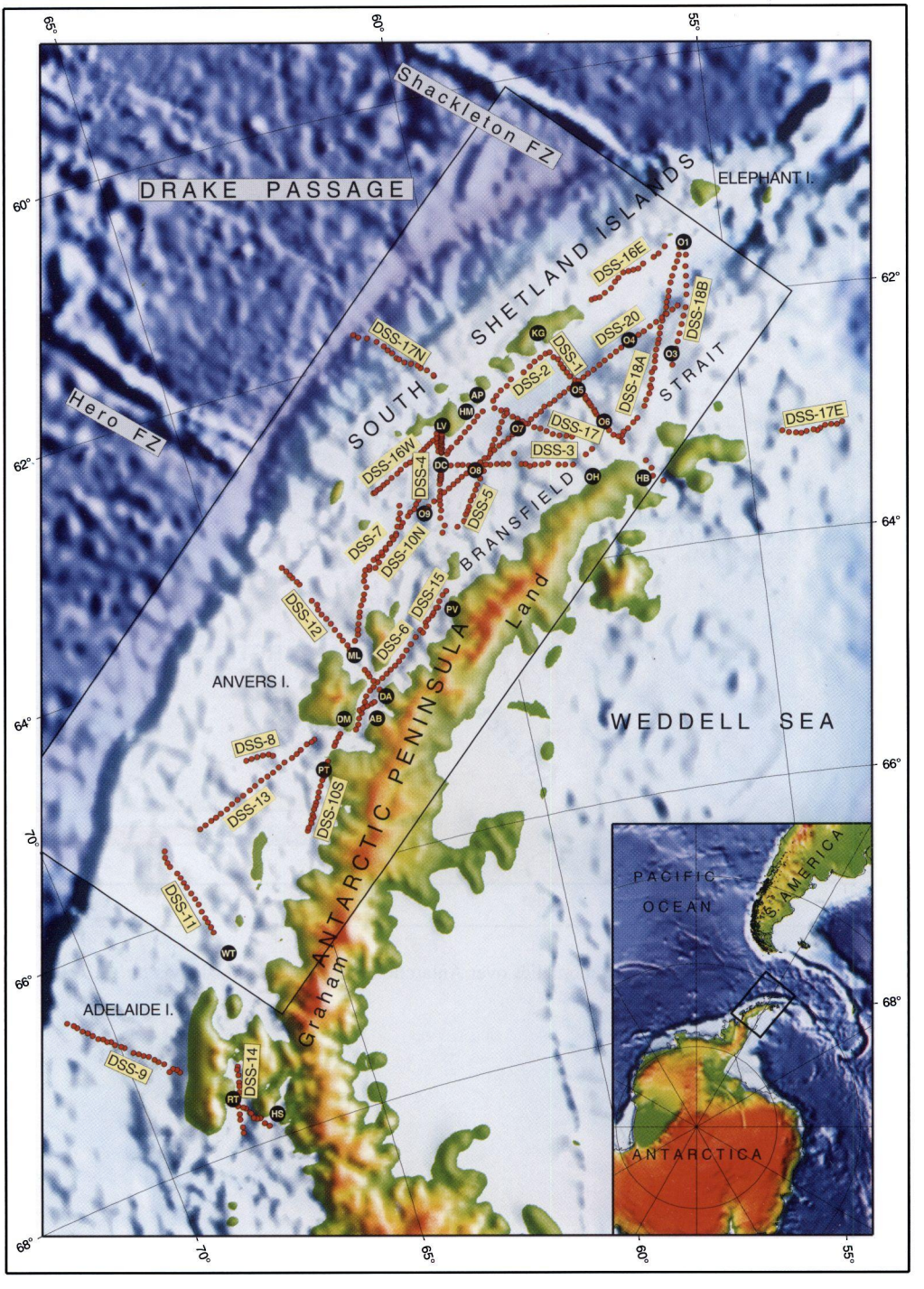

Fig. 1. Map of the study area. Shot locations are marked by red points, seismic stations are marked by black circles. Station DC is on Deception Island. The black rectangle shows the horizontal extent of the tomographic model.

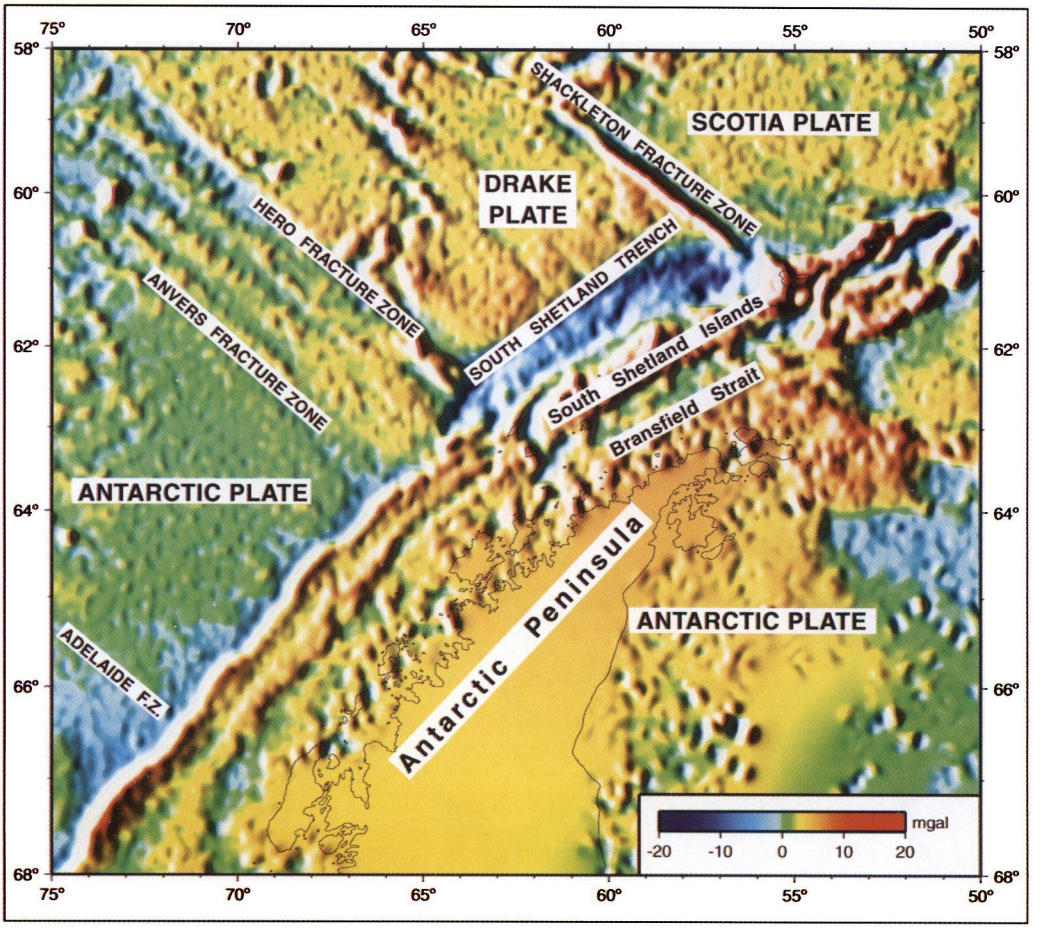

Fig. 2. Map of aeromagnetic anomalies over Antarctic Peninsula after Maslanyj *et al.* (1991).

tectonic histories. In the plate segment located between the Hero Fracture Zone and the Shackleton Fracture Zone, the oceanic Aluk ridge and the last segment of Aluk plate were preserved as the subduction stopped or slowed significantly about 4 Ma ago, before the ridge reached the margin (Henriet *et al.* 1992, Lawver *et al.* 1991).

Barker (1982) suggests that the end of subduction and spreading between HFZ and SFZ, together with continuing sinking of the subducted plate, might result in opening of the Bransfield Strait (1.3 Ma ago according to Roach (1978)) due to extensional forces.

The oceanic crust of the Pacific Ocean, adjacent to the margin, belongs to the Antarctic plate and is fragmented by several prominent fracture zones, approximately perpendicular to the margin: Tula FZ (north of Alexander Island), Adelaide FZ, Anvers FZ, Hero FZ and Shackleton FZ (south of South Shetland Islands), which define several plate segments (Fig. 2) (Anderson *et al.* 1990, Larter and Barker 1991). The extensions of the Hero FZ and Shackleton FZ on the shelf delimit the South Shetland Islands microplate, separated from the Antarctic Peninsula by the rift basin of the Bransfield Strait and bounded from NW by the subduction zone along the South Shetland trench. Off the South Shetland trench, between Hero FZ and Shackleton FZ, the last fragments of Drake plate (the last remaining fragment of partially subducted Aluk plate) and Aluk oceanic ridge, active until recent times, are preserved (Henriet *et al.* 1992).

Paleozoic basement under the Antarctic Peninsula is covered by Mesozoic/Cenozoic accretionary complex rocks and calc-alkaline plutonic and volcanic rocks. They are located on a fragment of continental crust and are built mainly of the Paleozoic and Mesozoic subduction complex created as the result of the accretion at the margin, later intrusion of Late Mesozoic and Cenozoic subvolcanic plutonic rocks (Barker and Dalziel 1983) and, finally, Pliocene to Recent magmatism due to the back-arc spreading.

Over the shelf area several elongated fore-arc basins were detected by seismic reflection measurements (Anderson *et al.* 1990, Henriet *et al.* 1992) and by refraction modelling (Środa *et al.* 1997). The basins are filled with volcanic mudstones and sandstones, covered by glacial and glacial-marine sediments. The basins are separated from the outer shelf area by a mid-shelf high (Larter and Barker 1991). These structures may represent an ancient back-arc basin and an eroded island arc, respectively (Gamböa and Maldonado 1990).

The Bransfield Strait contains a back-arc basin with a Late Cenozoic extensional grabenlike structure called the Bransfield rift (Birkenmajer 1992). The rift and the islands are located between the extensions of the Hero FZ and Shackleton FZ, which delimit also the remaining segments of the Aluk ridge. The sedimentary cover consists mainly of glacial-marine sediments: organic-rich hemipelagic sediments and glacially eroded terrigenous sediments (Jeffers and Anderson 1990).

In the rift zone, volcanic activity is observed along the volcanic ridge at the stratovolcano of Deception Island and several submarine volcanos (Saunders and

Tarney 1982). The composition of the volcanic rocks is intermediate between basalts typical for ocean ridges (Weaver *et al.* 1979) and calc-alkaline magmas common for early phase of back-arc spreading.

Geophysical data

The results of gravity measurements carried out by the British Antarctic Survey from 1959 in the Antarctic Peninsula region were described by Davey (1972), Renner *et al.* (1985) and Garrett (1990). Along the axis of the Antarctic Peninsula negative gravity anomalies are observed, with –10 to 0 mGal values over Graham Land. Elongated positive anomalies in 10–80 mGal range occur on the shelf between Adelaide and Anvers Islands. The Bransfield Strait area is characterized by positive Bouguer anomalies with complex pattern: a local gravity high (100–130 mGal) coinciding with South Shetland Islands, a maximum of 150 mGal in the NE part of the Bransfield Strait caused by shallow high density material (Davey 1972), and local minima over Deception Island and SW Bransfield Strait. In the Drake Passage over the South Shetland Islands shelf, an elongated local minimum exists that is probably caused by thick layer of low density sediments and relatively thick crust.

The studies of magnetic anomalies over the northern Antarctic Peninsula are based on the British Antarctic Survey data from aeromagnetic and marine magnetic profiles (Maslanyj *et al.* 1991). Over the South Shetland Islands, Graham Land and near Anvers Island, negative magnetic anomalies with amplitudes reaching –700 nT are observed. The whole area of the Scotia arc is characterized by linear belts of positive magnetic anomalies along the continental areas of the arc. The most prominent anomaly, extending for about 1300 km along the Antarctic Peninsula coast, is called the West Coast Magnetic Anomaly (WCMA) (Renner *et al.* 1982). The WCMA is about 50–100 km wide, with average anomaly amplitude of about 500 nT. High magnetic gradients are observed along its margins. The eastern portion of the WCMA is located offshore southern Graham Land and in the Bransfield Strait, and its maximum amplitude is 900 nT. The western portion has a maximum exceeding 1000 nT in the area NW of the South Shetland Islands. Both components are adjacent in the south, while in the north they are separated by the South Shetland Islands archipelago.

According to Garrett *et al.* (1986/1987) and Garrett and Storey (1987), the WCMA is caused by a long batholith of mafic to intermediate composition. The correlation of WCMA with positive gravity anomalies (Renner *et al.* 1985), and the information about the surface geology supports this interpretation. Garrett and Storey (1987) suggest that the batholith might be formed during Early Tertiary intra-arc extension by several intrusions of mafic and intermediate material. Later extension in the Bransfield Strait about 2 Ma ago split the northern part of the batholith in two parallel components.

First refraction surveys in the Antarctic Peninsula region were carried out by the British Antarctic Survey in the sixties. Cox (1964) interpreted the data from 5 refraction lines in the NE Bransfield Strait and found anomalously high velocity (6.4–7.1 km/s) at shallow depth (about 5 km). Ashcroft (1972) describes the results of the refraction survey in the Bransfield Strait. His model of the seismic wave velocities up to the depth of about 25 km shows significant variability of the crustal structure when moving from the Antarctic Peninsula through the Bransfield Strait and the South Shetland Islands to the Drake Passage. The upper crust beneath the Antarctic Peninsula shows relatively low P-wave velocities (6.2 km/s up to 20 km depth), indicating a typical continental character for the crust. Along the central part of the Bransfield Strait the crust consists of 2.5 km thick sediments, a 1 km thick layer of acidic crystalline rocks with V_P in the range of 5.3–5.6 km/s, and a 10 km thick layer of basic rocks with V_P equal to 6.6 km/s. Below these layers, at 15 km depth, the P-wave velocities of 7.7 km/s have been found. The crustal structure of the South Shetland Islands is similar to that of the Antarctic Peninsula. In the Drake Passage, NW of the South Shetland Islands, a 12 km thick oceanic crust has been found. On the basis of the geological data and of the modelling results, Ashcroft suggested that until Tertiary times, the South Shetland Islands and the Antarctic Peninsula formed one crustal block, and were separated when rifting started, opening the Bransfield Strait.

The results of seismic experiments carried out by Polish expeditions provided new information on the crustal structure of the passive continental margin of the Antarctic Peninsula south of the Hero Fracture Zone and in the Bransfield Strait. The 2-D modelling of the crustal structure in the Bransfield Strait and its vicinity was the subject of numerous papers (Guterch *et al.* 1985, Guterch *et al.* 1991, Grad *et al.* 1993, 1997; Janik 1997a). Results of the modelling allow to distinguish between different types of crust in separate crustal blocks: the continental crust beneath the Antarctic Peninsula, about 40–45 km thick with thin sedimentary cover and three crystalline layers with velocities of 5.5, 6.6 and 7.2 km/s; the thinner continental block of South Shetland Islands with a similar velocity structure, but shallower Moho depth (30–35 km); 12 km thick oceanic crust in the Drake Passage NW of South Shetland Islands; and anomalous crust in the Bransfield Strait, characterized by the occurrence of a high velocity body with velocities exceeding 7.4 km/s in the 14–30 km depth range, and Moho boundary at 30 km depth.

According to Środa *et al.* (1997) and Guterch *et al.* (1998), the Earth's crust beneath the Antarctic Peninsula south of the HFZ is continental in character. This is justified by the information about the P-wave velocity distribution and crustal thickness. Thickness of the sedimentary cover varies from 0.2–1.5 km in the coastal area to 5 km in the sedimentary basins on the continental shelf. The seismic velocities can be divided into three classes: 6.3–6.4, 6.6–6.8 and 7.1–7.2 km/s. The thickness of the crust varies from 36 to 42 km with maximum thicknesses below the Adelaide, Biscoe and Anvers Islands. A decrease of crustal thickness to about 25–28 km is observed towards the Pacific Ocean.

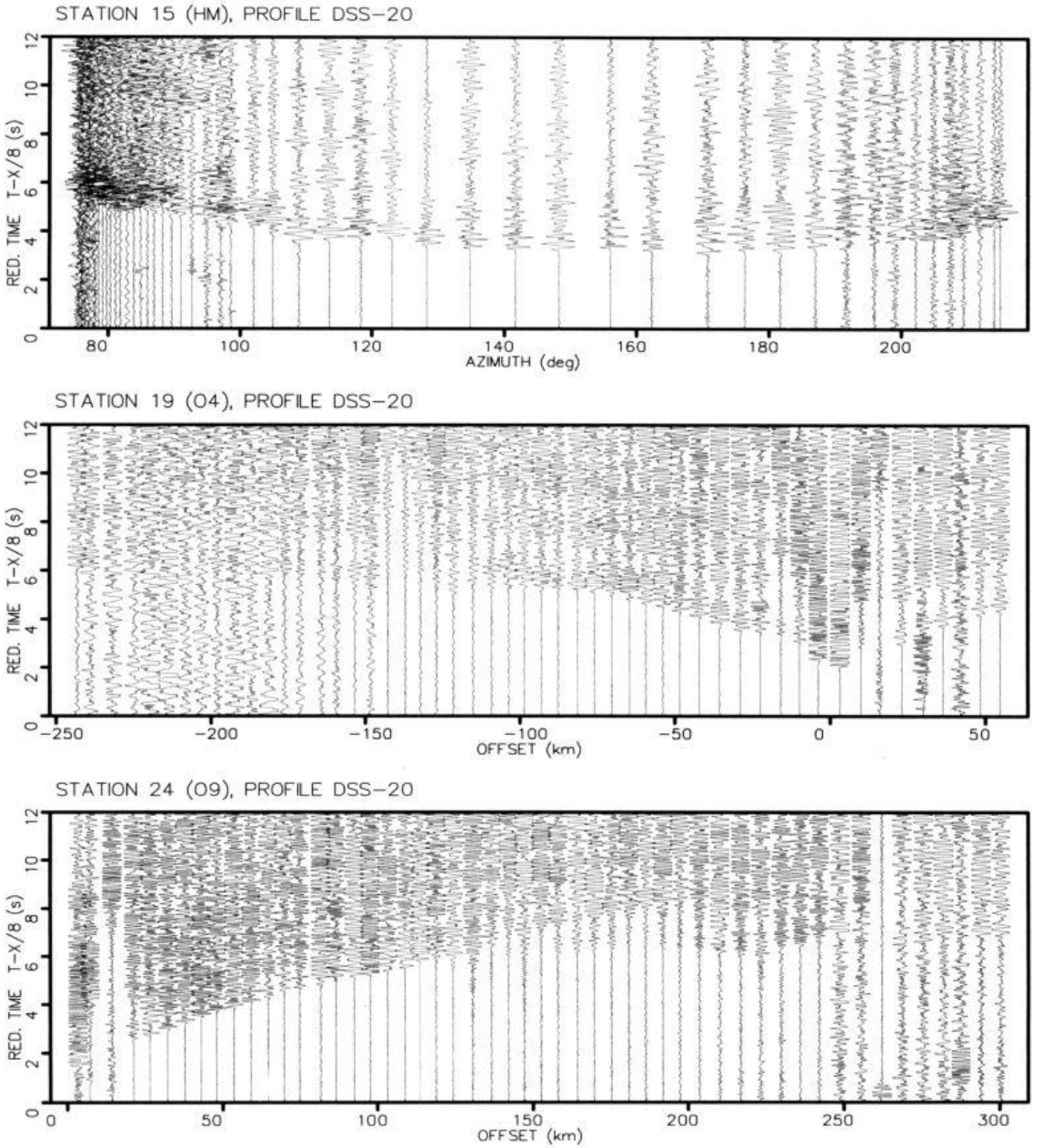

Fig. 3. Seismic record sections from profile DSS-20: station 15 (fan recordings), station 19 and station 24. Reduction velocity is 8 km/s, sections are normalized to maximum trace amplitude.

Seismic data and input data for inversion

The seismic data acquired during all Polish Antarctic expeditions consisted of about 2450 seismograms. The seismic records from land stations consist usually of 3 or 5 channels, recorded at approximately 200 m intervals. The data recorded by

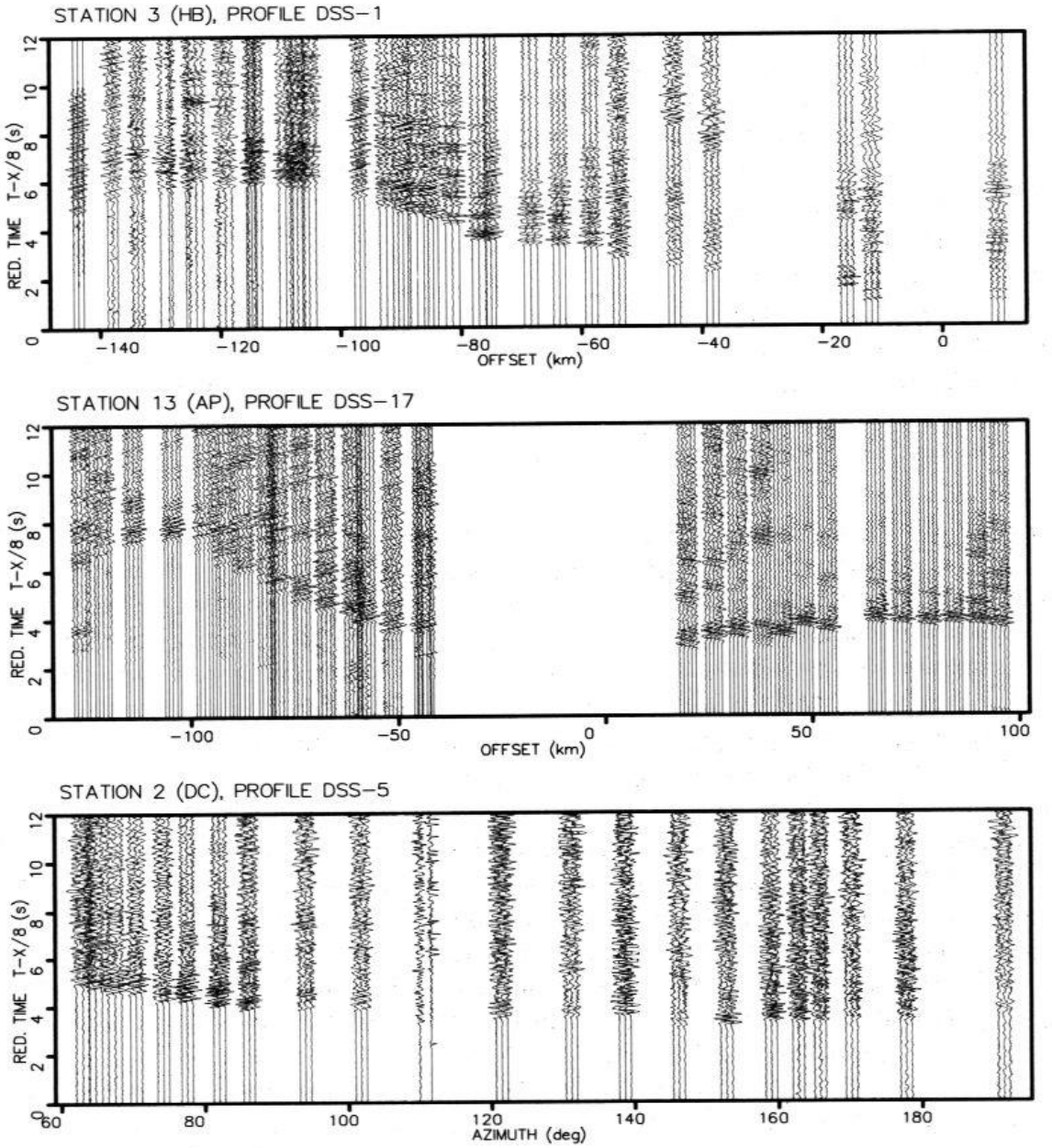

Fig. 4. Seismic record sections from Bransfield Strait and Drake Passage: station 3, profile DSS-1; station 13, profile DSS-17 and station 2, profile DSS-5 (fan recordings). Reduction velocity is 8 km/s, sections are normalized to maximum trace amplitude.

OBSs are single-channel. In case of multichannel recordings, the traveltime of the central channel was picked and used for the inversion.

Examples of the seismic data are shown in Figs 3, 4 and 5. Most of the seismic sections show good quality first arrivals in the whole offset interval.

The seismic P-wave field in the study area shows highly varying character. In the area north of the Hero Fracture Zone (the Bransfield Strait), the first arrivals show

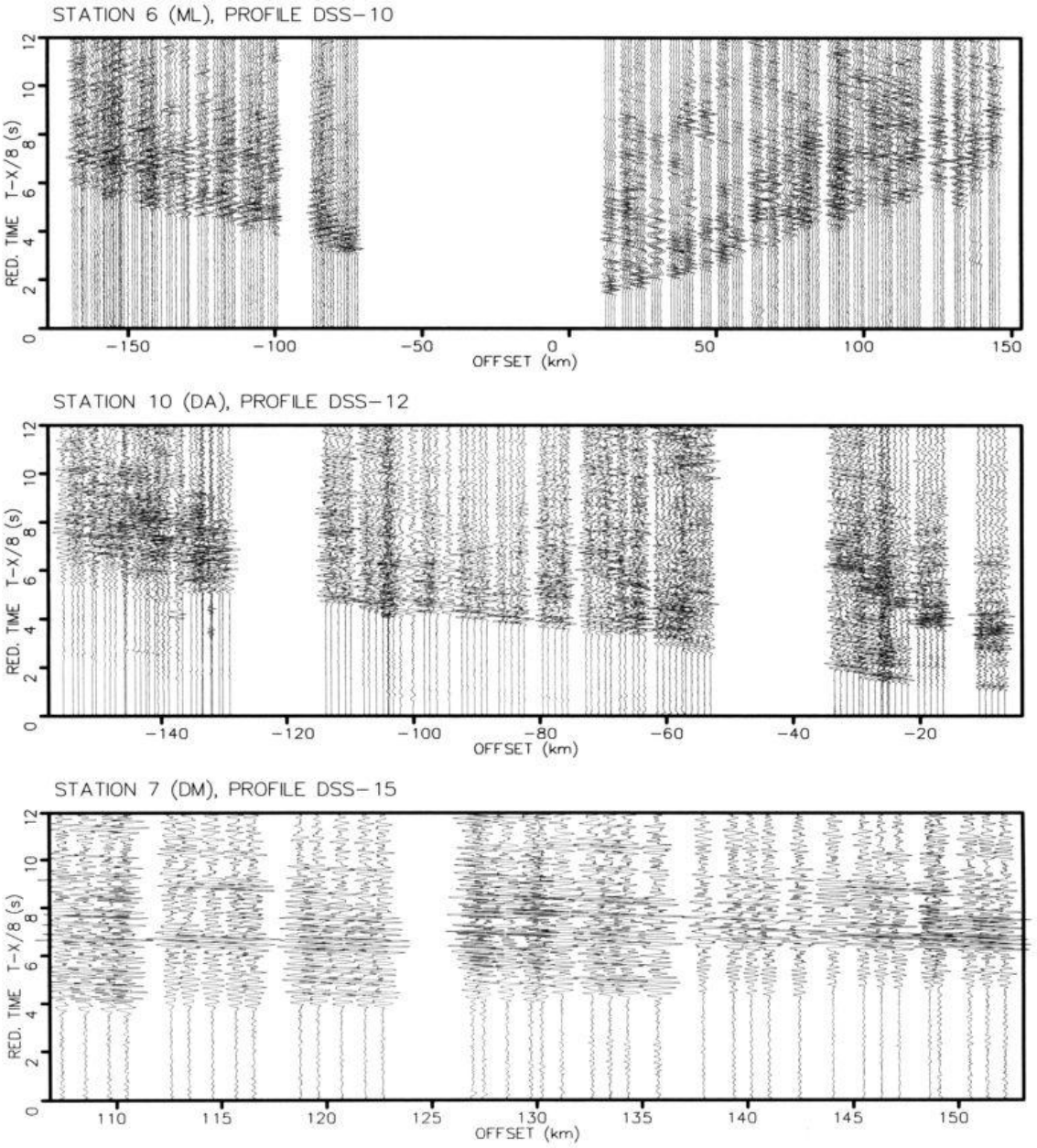

Fig. 5. Seismic record sections from Anvers Island region: station 6, profile DSS-10; station 10, profile DSS-12 and station 7, profile DSS-15. Reduction velocity is 8 km/s, sections are normalized to maximum trace amplitude.

generally higher apparent velocity and higher intercept time than sections from the area south of the Hero Fracture Zone. This indicates a thicker sedimentary layer and higher P-wave velocities in the middle and lower crust in the Bransfield Strait area.

The data from the Bransfield Strait prove the complexity of the crustal structure, sediment distribution and bathymetry in this area. On the seismic sections from profile DSS-20 (Fig. 3), situated along the axis of the Bransfield Strait, appar-

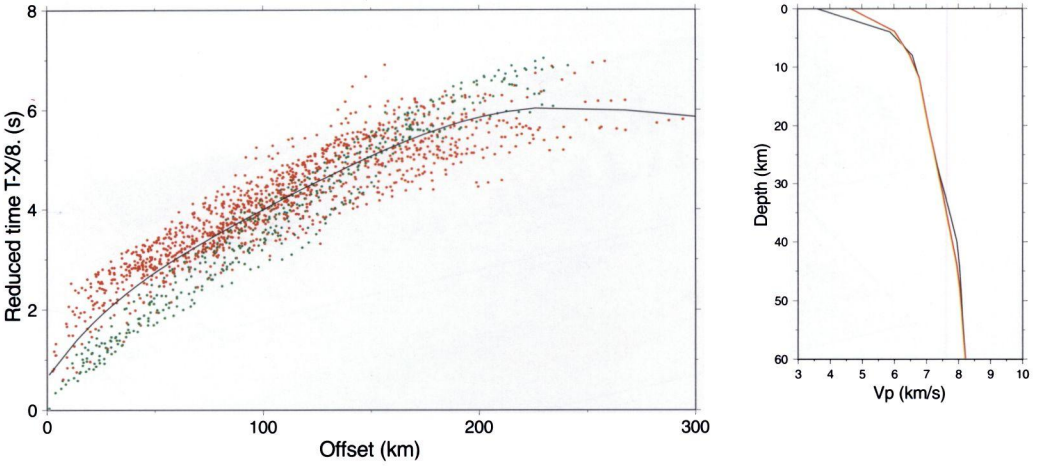

Fig. 6. Left: first arrivals data used for inversion (total 1670 points). Red points – traveltimes from the area north of HFZ, green points – traveltimes from the area south of HFZ. Corresponding average traveltime curves are shown (black curve is the average for all picks). Right: average 1-D model. Black line – calculated 1-D model, red line – smoothed model used as the initial model.

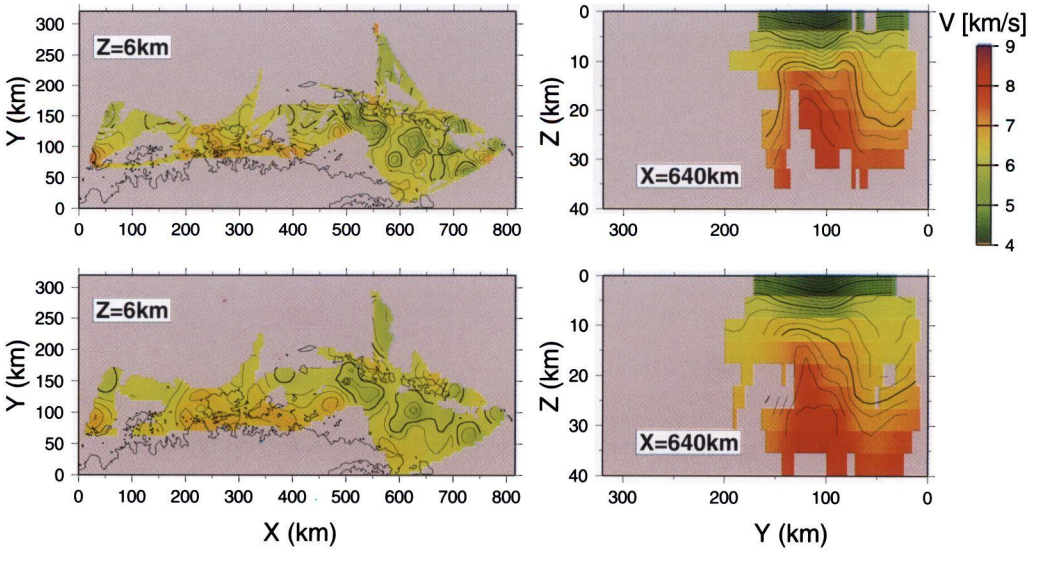

Fig. 7. Comparison of inversion results for IBP method (top) and RI method (bottom). Left: horizontal slices at 6 km depth, right: vertical slices at X = 640 km (Bransfield Strait). The interval of thick and thin velocity isolines is 1 km/s and 0.2 km/s, respectively.

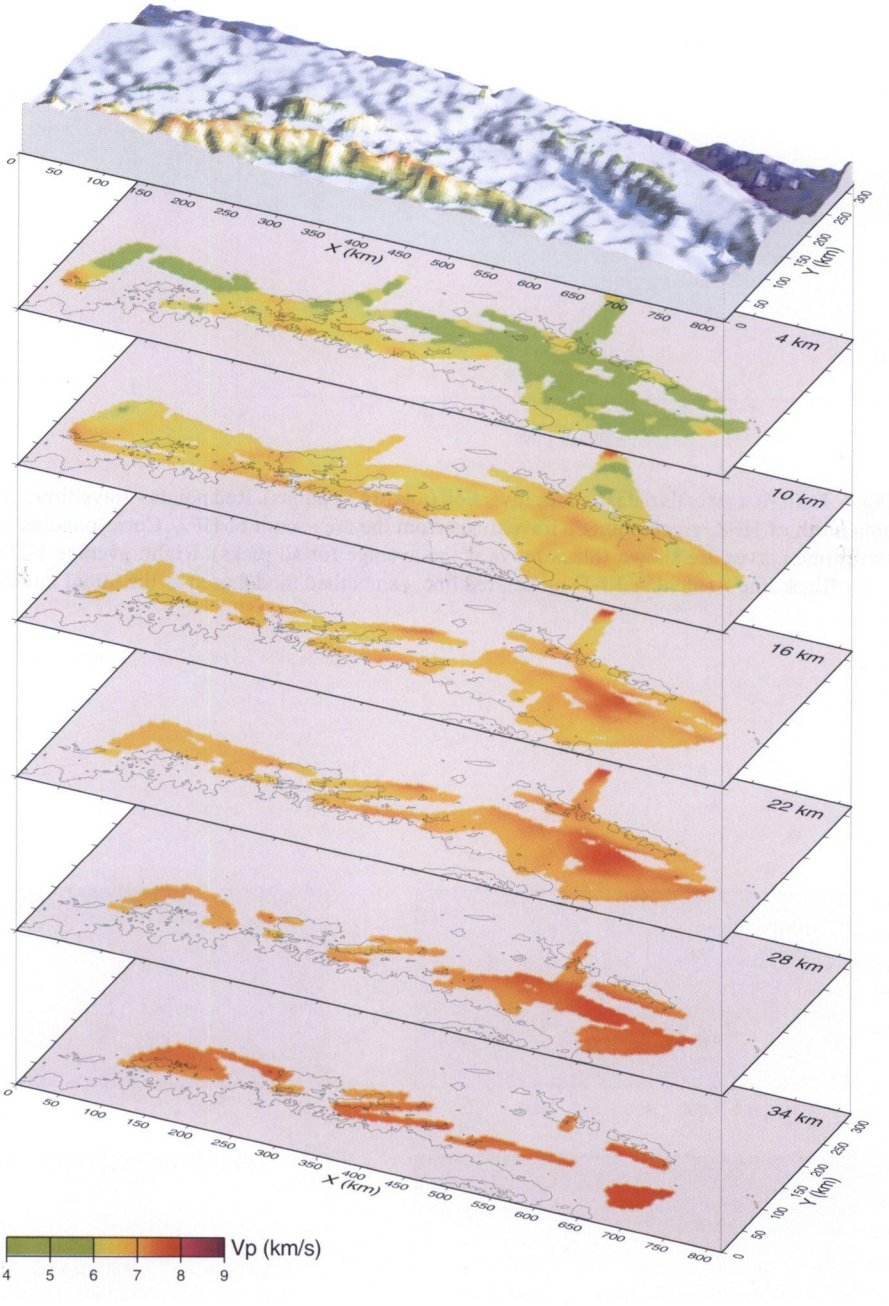

Fig. 8. Topography and horizontal slices through the V_P velocity distribution.

ent velocities of 6.10–6.30 km/s are observed. At larger offsets (from 80–120 km) the first arrivals show high (7.6–7.8 km/s) apparent velocities. The traveltime curve is regular and smooth. This is not the case for seismic sections from profiles situated perpendicular to the axis (e.g. DSS-1 and DSS-17 in Fig. 4), where the apparent velocity of first arrivals changes abruptly, reflecting changes of water depth and crustal structure in this direction. On the section for profile DSS-17 and station AP (Fig. 4) the apparent velocity of first arrivals in the Bransfield Strait (offset range 30–100 km) changes from 6.7 to 8.0 km/s. In the profile fragment located NW from the South Shetland Islands (offsets 50–140 km) the apparent velocity changes abruptly from 5.2 to 10 km/s. The recordings from profile DSS-1, Station HB, show apparent velocities of about 6.2 km/s (offsets 10–80 km), 5.0 km/s (offsets 80–110 km) and about 9.2 km/s (offsets 110–150 km).

The data collected in the area south of the Hero Fracture Zone (from Anvers Island to Adelaide Island) do not show such irregularities (Fig. 5). It is interesting that for almost all sections (except the profile DSS-9) only the P_g wave is visible in first arrivals in the whole offset interval (up to 230 km). Phases with apparent velocity of km/s, which could be interpreted as a P_n wave, are practically not observed. This is an indicator of a large crustal thickness. Because of the lack of arrivals refracted at the Moho discontinuity, the thickness of the crust can be estimated only using the information from reflected arrivals. Generally, refracted arrivals at offsets to about 100 km have relatively high apparent velocity of 6.3–6.4 km/s. At larger offsets, velocities of about 6.7–6.8 km/s are dominant. In the distance interval from 80 to 170 km, reflected waves with maximum amplitudes at 100–140 km were found. They are interpreted as reflections from the Moho boundary.

The input data for the inversion procedure were collected from all seismic sections with good signal-to-noise ratio by manual picking of the first onsets. A correction removing the effect of water layer on traveltimes has been applied to each trace start time before picking. All shot points and receivers are located at the flat upper boundary of the model, equivalent to the ocean bottom, and the depth of any point of the model is respective to the ocean floor, rather than ocean level. The correction has been applied because one of the inversion packages does not allow for defining an interface above which the velocity is held fixed, as it is usually done in order to simulate the water layer.

Input data for the tomographic inversion consisted of 1670 picked traveltimes of first arrivals. Fig. 6 shows first arrivals picks divided in two groups: picks from the region south of HFZ (Anvers Island) are plotted as green points, while the red colour marks picks from the area north of HFZ (Bransfield Strait and its vicinity). The plot shows clearly the difference of shape (slope and intercept time) for two groups of picks, suggesting strong lateral variability in crustal structure. Generally, high intercept time and lower slope for picks from the Bransfield Strait means thicker sedimentary layer and higher P-wave velocities in the middle and lower crust when compared to the southern part of the study area. Fig. 6 also shows the

mean traveltime curves, fitted to both groups of picks and to all picks together using least squares method. These curves were used for determination of the average velocity structure which served as the 1-D input model for inversion.

The uncertainty of the picked traveltimes has been estimated to be 0.1 s. The common procedure for removing picking errors in the case of seismic modelling using refracted waves from reversed shooting geometry is reciprocity checking. Unfortunately, it could not be applied here due to specific geometry of the experiment.

The initial model used in this work consists of a 1-D velocity distribution, calculated by 1-D trial-and-error modelling using an average traveltimes curve. The model obtained, shown as a black line, has been modified in order to decrease the velocity gradient in the first 4 km near the surface.

The velocity model has been defined in the rectangular area shown in Fig. 1. The dimensions of the model are km, with cell size of 4 km. Profiles DSS-9, DSS-14 and part of the profile DSS-17 were deliberately left outside the model because no off-line recordings were available and the ray coverage was poor and limited to the profile lines. In this way, substantial reduction of the model size has been obtained. The values were defined at the nodes of the cubic grid with spacing of 4 km.

Inversion method and modelling procedure

The tomographic inversion was carried out with two software packages applied to the same data set in order to compare both results. The iterative back-projection (IBP) package by Hole (1992) uses an efficient method of determining the seismic velocity distribution in a 3-D medium using first arrivals. The algorithm uses an approach of linearization of a non-linear relation between the traveltime t and the slowness u=1/v. The linearization results in an approximation:

$$\delta t = \int_{L[u0(r)]} \delta\, u(r)dl\,,$$

where δt is the traveltime perturbation, du is the slowness perturbation and u_0 is the reference slowness field and L is the integration path. The solution of the above equation is found iteratively. The model of the slowness field used for inversion is parametrized using a function defined along the ray path. This leads to the following solution for the slowness perturbation:

$$\delta u(r) = \begin{cases} \delta t_j / l_j & \text{for r along the path j;} \\ 0 & \text{otherwise} \end{cases}$$

By summing the reference model and perturbations we obtain a new reference model u_0. This procedure is repeated iteratively until a model with satisfying traveltime residuals is obtained.

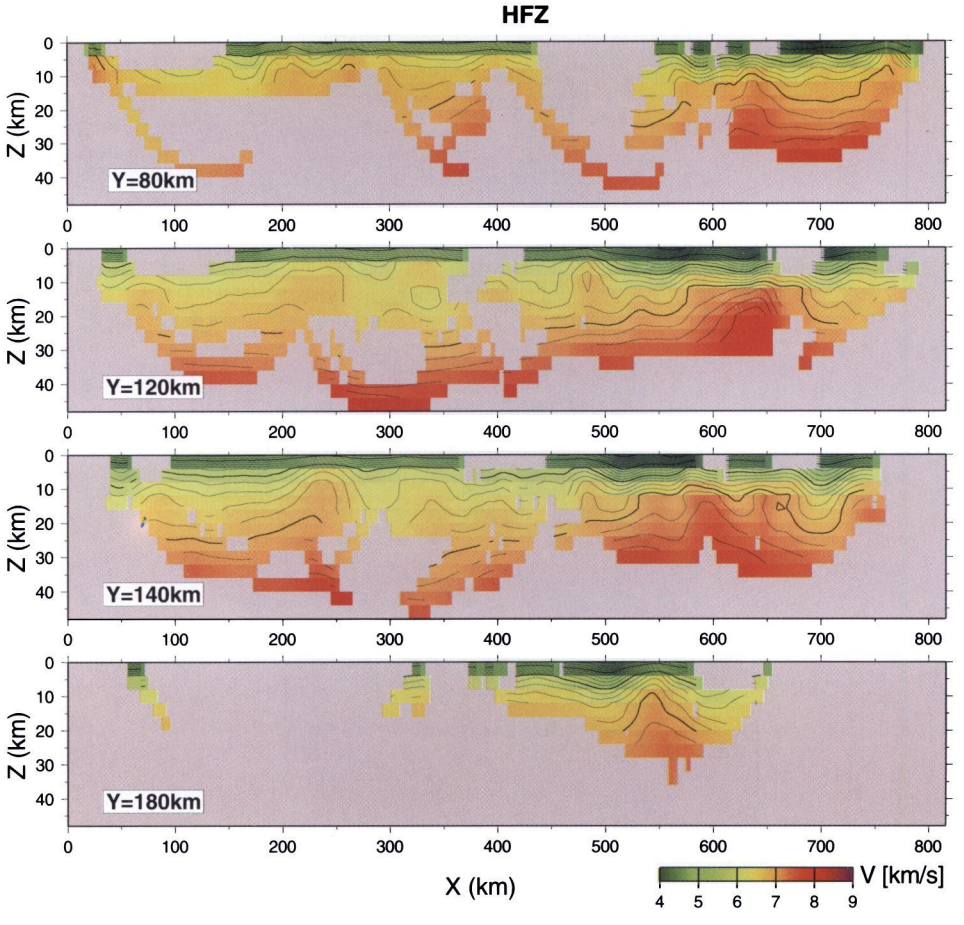

Fig. 9. Vertical slices in the Y-plane through the V_p velocity distribution. The interval of thick and thin velocity isolines is 1 km/s and 0.2 km/s, respectively.

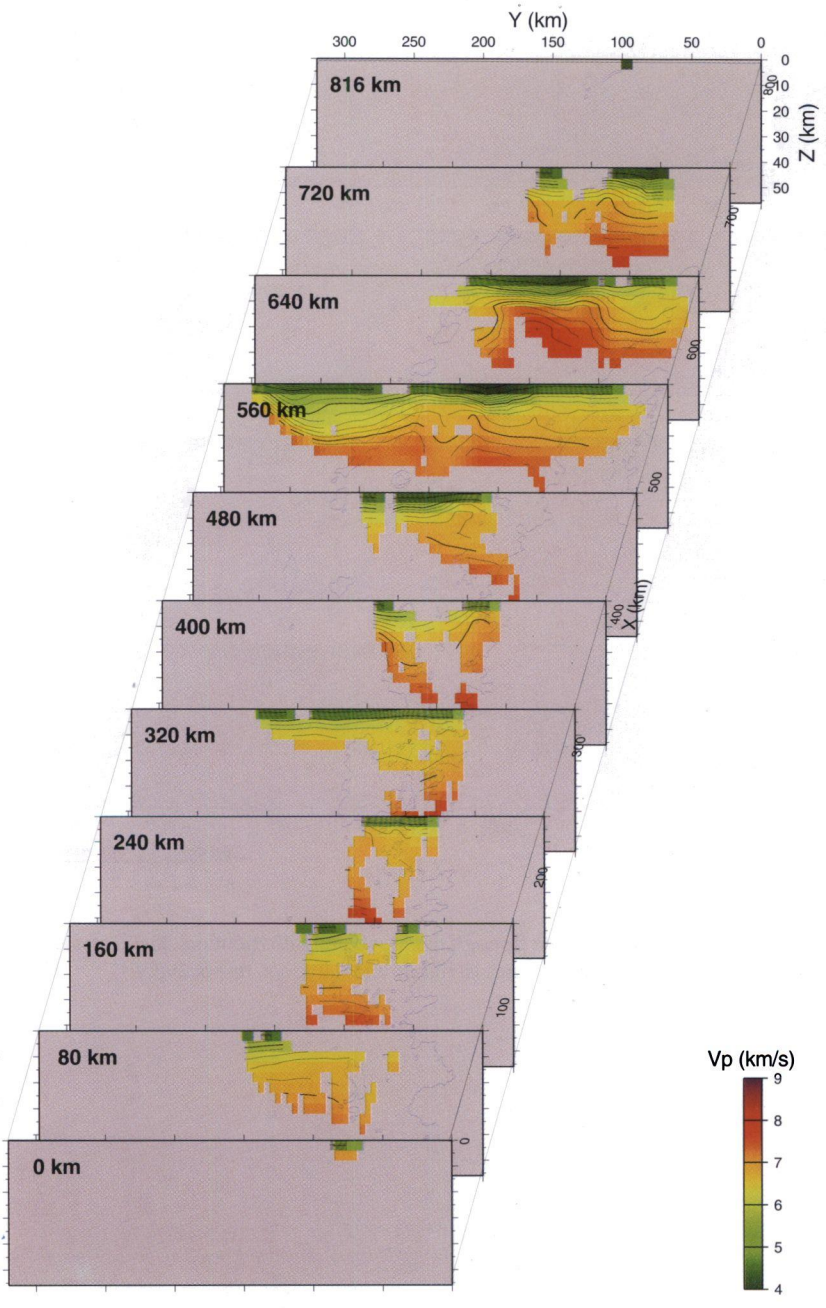

Fig. 10. Vertical slices in the X-plane through the V_p velocity distribution. The interval of thick and thin velocity isolines is 1 km/s and 0.2 km/s, respectively.

The velocity model is defined by the rectangular grid with equidistant nodes. The traveltimes are calculated using the finite differences algorithm by Vidale (1990) adapted for media with high velocity contrasts by Hole (1992). The ray paths are traced from the receivers back to the source along the maximum traveltime gradient curves.

The slowness perturbation in each grid node is calculated as an average of du in all nodes in a block around the given node. This procedure allows for the parametrization of du on an equidistant grid, and stabilizes the inversion by smoothing the velocity field.

Another program used in this work is the FAST package (Zelt and Barton, 1998). It implements the regularized inversion (RI) method with smallest roughness constraint. The solution of the inverse problem is sought iteratively. In each iteration, the algorithm minimizes a function which is a linear combination of the data misfit and the measure of the model roughness:

$$\Phi(\mathrm{m}) = \delta \mathrm{t}^{\mathrm{T}} \mathrm{C}_d^{-1} \delta \mathrm{t} + \lambda (\mathrm{m}^T \mathrm{C}_h^{-1} \mathrm{m} + \mathrm{s}_z \mathrm{m}^T \mathrm{C}_v^{-1} \mathrm{m}),$$

where δt is the traveltime residual vector, C_d is the data covariance matrix, C_h and C_v are finite difference operators measuring the horizontal and vertical model roughness, λ is the trade-off parameter weighting the importance of the roughness constraint and s_z determines relative weights of horizontal and vertical smoothing constraint.

The obtained slowness perturbation field δm is used to update the reference model and the new model is used as the input for next iteration step. In each iteration, different variants of model are calculated with different values of the trade-off parameter λ and the variant which produces the smallest data misfit is selected for next iteration. The algorithm attempts to find a solution producing RMS residual approximately equal to the level of data uncertainty. In the case when this condition is satisfied before the end of iterations sequence, the algorithm does not overfit the theoretical traveltimes to the data, but the smoothest/flattest possible model is sought.

The sequence of iterations for the IBP package has been designed to allow for gradual increasing of the thickness of the modelled area. In this way, early iteration steps resolved the near-surface structures before the deeper parts were modelled. The smoothness of the velocity distribution was decreased in the process. It stabilized the model in the beginning and allowed for gradual introduction of smaller-size structures. The iteration steps were run repeatedly in three nested loops: the innermost loop contains N iterations with constant parameters, middle loop is performed with decreasing values of smoothing operator size and in the outer loop the values of X_{max} (maximum offset of picks used for inversion) are increased. Total number of 30 iterations was used.

For the modelling using the RI package the velocity distribution is parametrized in a similar way as for IBP method. The modelling sequence consists of a

user-defined number of nonlinear iterations. For each iteration, several values of trade-off parameter λ are tested. The operator can set several inversion parameters concerning *e.g.* the overall smoothness or flatness of the model. Different values of these parameters were tried during synthetic tests and inversion of the real data. Optimal values were used for final modelling. Regularized inversion was performed with 3 nonlinear iterations and 7 λ values for each iteration, using the minimum smoothness constraint.

The description and interpretation of the velocity model

Selected slices from two versions of a final model were compared to check how the methods influence the result. Fig. 7 presents slices in the Z and X plane for model obtained with IBP package, and model obtained with RI package.

The models are essentially very similar when comparing location of large scale inhomogeneities and velocity distribution with depth. The only difference is in the minimum wavelength of observed inhomogeneities. The IBP model contains short-wavelength features (size of 50 km and smaller). They are mostly of no importance for interpretation, as their size is often below the estimated resolution. The RI model is smoother. The differences are in some degree due to the choice of the smoothing parameters in inversion procedures. The wavelength of the anomalies is larger than 50 km, approximately. Further discussion is based on the IBP model.

The final velocity distribution obtained with IBP package is shown in Figs 8, 9 and 10. The velocity model has been cut in 2-D slices in selected places in order to allow visual inspection of the 3-D volume. For horizontal slices in the Z-plane, velocity values for each node were plotted only if the ray density in the corresponding cell had non-zero value, in order to show only constrained areas. For vertical slices in the X and Y planes, the ray density in the 8 cells wide swath around the cutting plane was summed to create a mask used for finding the constrained areas in the given slice. This procedure is somewhat misleading, as the figures obtained in this way show better ray coverage than actual, but on the other hand it helps to present the velocity field without too many empty areas due to the fact that the slices are not parallel to the lines of seismic profiles.

The example diagram of the ray coverage is presentd in Fig. 11. In large parts of the constrained area the ray density is poor (1–2 rays per cell), which indicates that caution is needed in interpreting the results based on data with such spatial density of measurements.

The results of modelling reflect the complex structure of the Earth's crust in the study area and allow for determining the regions which underwent different tectonic and geological evolution.

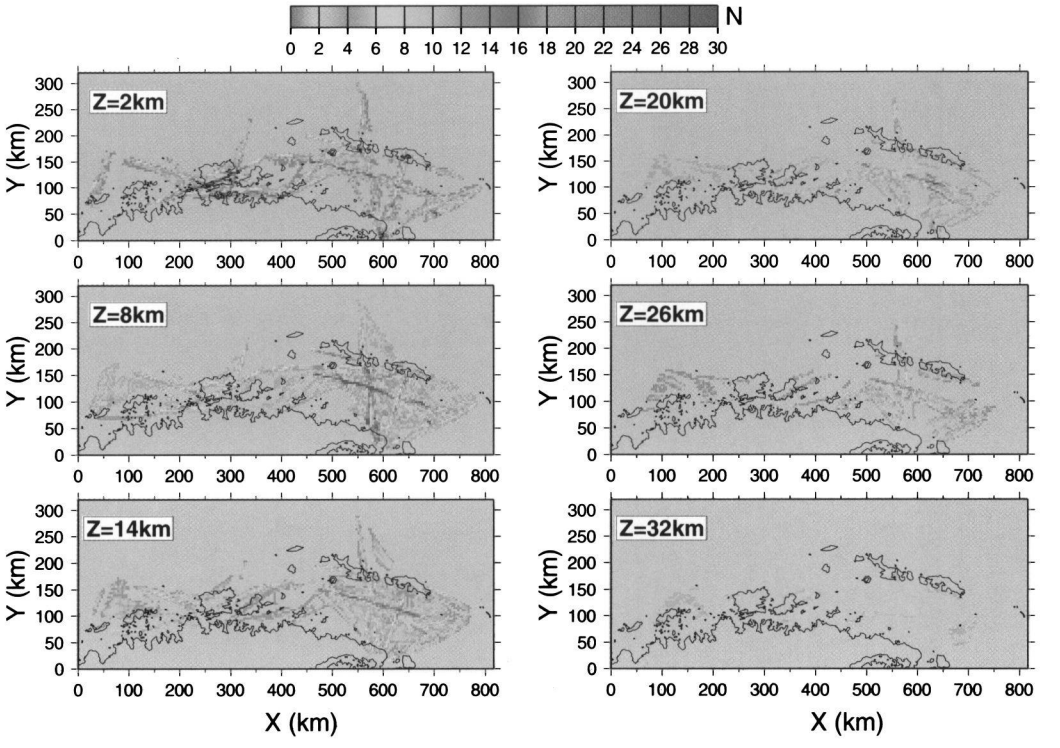

Fig. 11. Ray coverage at different depths.

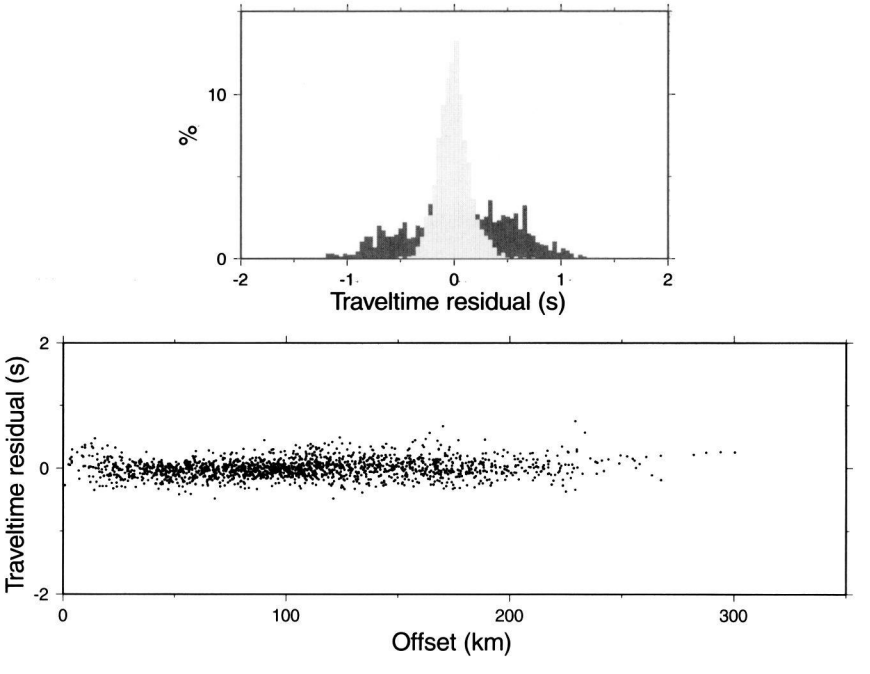

Fig. 12. Distribution of traveltime residuals (top) and dependence of traveltime residuals on offset (bottom) for IBP method. Dark bars are for the initial model, light bars – for the final model.

In the horizontal slices, low velocity areas with V_P less than 5.0 km/s at shallow depths correspond to sedimentary basins found previously along the Antarctic Peninsula shelf and in the Bransfield Strait by means of reflection and refraction seismics(Anderson *et al.* 1990, Henriet *et al.* 1992, Środa *et al.* 1997).

In the northern part of the Bransfield Strait at depth 16 km, an area of anomalously high velocity (7.4 km/s) is observed. The location of this area is consistent with the results of Janik (1997b), obtained by 2-D raytracing and trial-and-error seismic modelling. Extremely high velocities at shallow depth can be explained by the existence of large amounts of ultramafic mantle material that replaced the lower and middle crust, thinned during crustal extension.

The vertical slices in the Y-plane show clearly the difference in the crustal structure between the areas south and north of the extension of the Hero Fracture Zone. In the large parts of the Bransfield Strait, observed velocities are generally high for continental crust, especially in the high velocity anomaly area. Overall values of V_P are smaller in the vicinity of the Anvers Island south of the Hero Fracture Zone, where the velocity distribution is similar to normal continental crust, except of some areas of slightly higher velocity (6.5 km/s) at shallow depth in the coastal area (this may be caused by the existence of the mafic plutonic bodies along the Antarctic Peninsula postulated by Garrett *et al.* (1986/1987) to explain the West Coast Magnetic Anomaly).

The velocities of 8 km/s practically do not occur in the constrained area of the model. The highest value of V_P in the ray covered area is about 7.9 km/s. This is primarily caused by the absence of clear P_n phases, which would allow to determine the depth ot the Moho discontinuity. Phases with apparent velocity of more than 8 km/s were found only in some sections from the Bransfield Strait, but apparently they are not numerous enough to sufficiently constrain the deepest parts of the model. Moreover, modelling of strong velocity contrasts, as the Moho boundary, with tomographic algorithms described here is problematic.

Because of these limitations, the exact determination of the crustal thickness based on the inversion methods used is difficult. In the final model, variations in the crustal thickness can be observed taking into account the depth to the high velocities (7.6–7.8 km/s) areas. In the region south of the Hero Fracture Zone the crust is significantly thicker than in the Bransfield Strait area, with approximate thicknesses estimated to 40-45 km and 30 km or less, respectively. The crustal thickness beneath the South Shetland trench NW of South Shetland Islands is approximately 10 km.

Estimation of the errors, model resolution and quality

The calculation of the inversion model is usually followed by the model quality assessment using various methods. The methods used in this work in-

cluded: checking of RMS residuals and values, plots of RMS residuals distribution, calculating of the ray density distribution and dependence of the average ray density on depth, synthetic checkerboard tests (Zelt and Barton 1998), and inversion of Gaussian noise (Hole 1992). Only selected results of the above methods are presented.

As a general measure of the consistency of the final model and the data, the RMS traveltime residuals (RMS) were analysed. It describes the difference between the experimental traveltimes and theoretical traveltimes calculated for a given model. The RMS values for final IBP and RI models are 0.15 s and 0.14 s. These values exceed the assumed level of noise in the data – 0.1 s. This may mean that the level of the noise has been underestimated, and in reality it is probably at about 0.15 s. This is probably due to timing and location inaccuracies and to the lack of reciprocity checking, which would help to reduce data inconsistency.

The diagrams of traveltime residual distribution (an example for the IBP method is shown in Fig. 12) give more detailed information about the quality of data fit. Histograms of RMS values for initial and final models are shown, as well as the dependence of the RMS values on the offset. Both histograms are centered on the zero value and show substantial improvement of the fit compared to the initial distribution of residuals (green bars). The RMS values are more or less regularly distributed in the whole offset interval, what means that the errors are not due to some specific group of arrivals.

The ray coverage of the final model obtained by IBP method (the coverage for RI model does not show significant difference) presented in Fig. 11 is highly inhomogeneous, as shotpoints and receivers were spaced irregularly. Moreover, rays are concentrated mainly along the profiles, as the experiments were oriented primarily for 2-D modelling. The ray coverage depends strongly on depth, reaching a maximum at 8–12 km. The ray coverage is best in the area of the Bransfield Strait and in the vicinity of Anvers Island, because of high concentration of shot points and receivers in these areas.

The test of inversion of the Gaussian noise shows that the synthetic data with uncertainty of 0.15 s produce the model with velocity fluctuations with average amplitude of the order of 0.06 km/s. This value is an average for the whole model – the amplitude varies with depth and location in the model. This test does not take into account other factors affecting the uncertainty of the velocity distribution that are difficult to estimate.

The resolution tests showed that the horizontal resolution of the model is highly variable and depends on the ray density. In almost whole constrained model area, the tomographic modelling can detect inhomogeneities of about 100 km size or smaller. In the area with good ray density (the central part of the Bransfield Strait) at moderate depth (less than about 15 km) crustal structures of 50 km size can be resolved. The resolving capability of the method decreases strongly with depth.

Conclusions

- Tomographic inversion of 1670 first arrival traveltimes produced a velocity distribution model down to about 40 km depth. The cell size of 4 km has been considered optimal for given geometry of survey and shots/stations density. The main results of the modelling are as follows:
- At depths down to 8 km, the areas with P-wave velocity less then 6 km/s were observed. They correspond to sedimentary basins in the area of Antarctic Peninsula shelf and in the Bransfield Strait.
- Relatively high velocities (6.3–6.5 km/s) occur at depths of 5–10 km in the coastal area, coinciding with the location of positive aeromagnetic anomalies (WCMA).
- An area of anomalously high velocities (more than 7.4 km/s) was found at depths of 16 km and deeper in the northern part of the Bransfield Strait. This confirms previous results of 2-D forward modelling and provides more information about the extent of the high velocity area.
- The crustal thickness south of the HFZ extension is estimated to 40–45 km. North of the HFZ extension, in the Bransfield Strait area, characterized by generally high velocities, the crust is thinner and probably does not exceed 30 km. The crustal thickness under the South Shetland trench was estimated to about 10 km.
- Obtained model is consistent with results of previous seismic research, mainly 2-D modelling, as well as with the distribution of magnetic and gravity anomalies, described earlier in this paper. Moreover, application of 3-D modelling method to the data from off-line recordings allowed for more detailed determination of the crustal structure in areas covered by dense network of profiles, mainly in the Bransfield Strait. The results clearly show the continental character of the Earth's crust beneath the Antarctic Peninsula and South Shetland Islands. The results confirm also the tectonic view of the Bransfield Strait as a rift basin with prominent sedimentary cover and anomalous crust, thinned and underplated by high velocity ultramafic material during extensional processes.
- The inversion methods applied in this study allows for assessment of the model uncertainty and resolution, what is a substantial advantage when compared to trial-and-error methods. Another advantages of the method is that if new traveltime data are acquired in future surveys, they can be easily incorporated into the existing data set and inverted jointly. In this way, a new velocity model can be created using all available information.
- Presented results were obtained using only a part of the collected traveltimes data – the traveltimes of first arrivals of seismic waves. Future incorporation of the reflected wave arrivals in the inversion procedure will significantly enhance of the velocity model. In particular, it will allow for more exact determination of the velocity distribution of the lower crust and of the Moho depth.

Acknowledgements. — All maps and slices of the 3-D models were plotted using the GMT 3.2 package (Wessel and Smith 1998).

References

ANDERSON J.B., POPE P.G. and THOMAS M.A. 1990. Evolution and hydrocarbon potential of the northern Antarctic Peninsula continental shelf. — *In:* St. John B. (ed.), *Antarctica as an exploration frontier.* American Association of Petroleum Geologists, Tulsa, Oklahoma, 31: 1–12.

ASHCROFT W.A. 1972. Crustal structure of the South Shetland Islands and Bransfield Strait. — British Antarctic Survey Scientific Reports, 66: 1–43.

BARKER P.F. 1982. The Cenozoic subduction history of the Pacific margin of the Antarctic Peninsula: ridge crest – trench interactions. — Journal of the Geological Society of London, 139: 787–801.

BARKER P.F. and DALZIEL I.W.D. 1983. Progress in geodynamics in the Scotia Arc region. — *In:* Cabr R. (ed.), *Geodynamics of the Eastern Pacific Region, Carribean and Scotia Arcs.* — Geodynamics Series American Geophysical Union Series, Washington, DC, 9: 137–170

BIRKENMAJER K. 1992. Evolution of the Bransfield basin and rift, West Antarctica. — *In*: Yoshida Y. *et al.* (ed.), *Recent Progress in Antarctic Earth Science*; 405–410.

COX M.J.G. 1964. Seismic refraction measurements in Bransfield Strait. — British Antarctic Survey Bulletin, 4: 1–12.

DAVEY F.J. 1972. Marine gravity measurements in Bransfield Strait and adjacent areas. *In*: Adie R.J. (ed.), *Antarctic Geology and Geophysics. Universitetsforlaget*, Oslo; 39–47.

GAMBÔA L.A.P. and MALDONADO P.R. 1990. Geophysical investigation in the Bransfield Strait and Bellingshausen Sea, Antarctica. *In*: St. John B. (ed.), *Antarctica as an exploration frontier. American Association of Petroleum Geologists*, Tulsa, Oklahoma, 31: 127–141.

GARRETT S.W. 1990. Interpretation of reconnaissance gravity and aeromagnetic surveys of the Antarctic Peninsula. — Journal of Geophysical Research, 95: 6759–6777.

GARRETT S.W., RENNER R.G.B., JONES J.A. and MCGIBBON K.J. 1986/1987. Continental magnetic anomalies and the evolution of the Scotia Arc. — Earth and Planetary Science Letters, 81: 273–281.

GARRETT S.W. and STOREY B.C. 1987. Lithospheric extension on the Antarctic Peninsula during Cenozoic subduction. — *In*: Coward M.P., Dewey J.F., and Hancock P.L. (eds), *Continental Extensional Tectonics*. Spec. Publ. Geol. Soc. London, 28: 419–431.

GRAD M., GUTERCH A. and JANIK T. 1993. Seismic structure of the lithosphere across the zone of subducted Drake plate under the Antarctic plate, West Antarctica. — Geophysical Journal International, 115: 586–600.

GRAD M., GUTERCH A. and ŚRODA P. 1992. Upper crustal structure of Deception Island area, Bransfield Strait, West Antarctica. — Antarctic Science, 4: 469–476.

GRAD M., SHIOBARA H., JANIK T., GUTERCH A. and SHIMAMURA H. 1997. Crustal model of the Bransfield Rift, West Antarctica, from detailed OBS refraction experiments. — Geophysical Journal International, 130: 506–518.

GUTERCH A., GRAD M., JANIK T. and PERCHUĆ E. 1991. Tectonophysical models of the crust between the Antarctic Peninsula and the South Shetland trench. — *In*: Thomson M.R.A., Crame J.A., and Thomson J.W. (eds), *Geological Evolution of Antarctica.* Fifth International Symposium on Antarctic Earth Sciences, Cambridge University Press; 499–504.

GUTERCH A., GRAD M., JANIK T., PERCHUĆ E. and PAJCHEL J. 1985. Seismic studies of the crustal structure in West Antarctica 1979–1980 — preliminary results. –Tectonophysics, 114: 411–429.

GUTERCH A., GRAD M., JANIK T. and ŚRODA P. 1998. Polish Geodynamic Expeditions — seismic structure of West Antarctica. — Polish Polar Research, 19: 113–123.

HENRIET J.P., MEISSNER R., MILLER H. and the GRAPE Team 1992. Active margin processes along the Antarctic Peninsula. — Tectonophysics, 201: 229–253.

HOLE J.A. 1992. Nonlinear high resolution three-dimensional seismic travel time tomography. — Journal of Geophysical Research, 97: 6553–6562.

JANIK T. 1997a. Seismic crustal structure in the transition zone between Antarctic Peninsula and the South Shetland Islands. — *In*: Ricci C.A. (ed.), *The Antarctic Region: Geological Evolution and Processes*. Proceedings of the VII International Symposium on Antarctic Earth Sciences, Terra Antarctica Publication, Siena; 679–684.

JANIK T. 1997b. Seismic crustal structure of the Bransfield Strait, West Antarctica. — Polish Polar Research, 18: 171–225.

JEFFERS J.D. and ANDERSON J.B. 1990. Sequence stratigraphy of the Bransfield Basin, Antarctica: implications for tectonic history and hydrocarbon potential. — *In*: B.S. John (ed.), *Antarctica as an exploration frontier*. American Association of Petroleum Geologists, Tulsa, Oklahoma, 31: 13–21.

LARTER R.D. and BARKER P.F. 1991. Neogene interaction and glacial processes at the Pacific margin of the Antarctic Peninsula. — Spec. Publs. Int. Assoc. Sediment, 12: 165–186.

LAWVER L.A., ROYER J.-Y., SANDWELL D.T. and SCOTESE C.R. 1991. Evolution of the Antarctic continental margins. — *In*: Thomson M.R.A., Crame J.A., and Thomson J.W. (eds), *Geological Evolution of Antarctica*. Fifth International Symposium on Antarctic Earth Sciences, Cambridge University Press: 533–539.

MASLANYJ S.W., GARRETT S.W., JOHNSON A.C., RENNER R.G.B. and SMITH A.M. 1991. Aeromagnetic anomaly map of West Antarctica (Weddell Sea sector), sheet 2. BAS GEOMAP Series, British Antarctic Survey, Cambridge.

MENEILLY A.W., HARRISON S.M., PIERCY B.A. and STOREY B.C. 1987. Structural evolution of the magmatic arc in northern Palmer Land, Antarctic Peninsula. — *In*: McKenzie G.D. (ed.), *Gondwana Six: structure, tectonics and geophysics*: American Geophysical Union Geophysical Monograph, 40: 209–219.

RENNER, R. G.B., DIKSTRA B.J. and MARTIN J.L. 1982. Aeromagnetic surveys over the Antarctic Peninsula. — *In*: C. Craddock (ed.), *Antarctic Geoscience*. University of Wisconsin Press, Madison: 363–367.

RENNER R.G.B., L. STURGEON J.S. and GARRETT S.W. 1985. Reconnaissance Gravity and Aeromagnetic Surveys of the Antarctic Peninsula. — British Antarctic Survey Scientific Reports, 110: 1–54.

ROACH P.J. 1978. The nature of back-arc extension in Bransfield Strait. — Geeophysical Journal of the Royal Astronomical Society, 56: 165.

SANDWELL D.T. and SMITH W.H.F. 1997. Marine gravity from Geosat and ERS 1 satellite altimetry. — Journal of Geophysical Research, 102: 10039— 10054.

SAUNDERS A.D. and TARNEY J. 1982. Igneous activity in the southern Andes and nothern Antarctic Peninsula, a review. — Journal of the Geological Society, London, 139: 691–700.

ŚRODA P., GRAD M. and GUTERCH A. 1997. Seismic models of the Earth's crustal structure between the South Pacific and the Antarctic Peninsula. — *In*: Ricci C.A. (ed.), *The Antarctic Region: Geological Evolution and Processes*. Terra Antarctica Publication, Siena: 685— 689.

VIDALE J. E. 1990. Finite-difference calculation of travel times in three dimensions, — Geophysics, 55: 521–526.

WEAVER S.D., SAUNDERS A.D., PANKHURST R.J. and TARNEY J. 1979. A geochemical study of magmatism associated with the initial stages of back-arc spreading: the Quaternary volcanics of the Bransfield Strait from South Shetland Islands. — Contributions for Mineralogy and Petrology, 68: 151–169.

WESSEL P. and SMITH W.H.F. 1998. New, improved version of Generic Mapping Tools released. — EOS Trans. Amer. Geophys. U., 79: 579.

ZELT C.A. and BARTON P.J. 1998. Three-dimensional seismic refraction tomography: A comparison of two methods applied to data from the Faeroe Basin. — Journal of Geophysical Research, 103: 7187–7210.

Received January 25, 2001
Accepted April 23, 2001

Streszczenie

W pracy przedstawiono wyniki trójwymiarowego modelowania struktury skorupy ziemskiej w rejonie Półwyspu Antarktycznego (fig. 1–2). Wykorzystano materiały z 21 profili sejsmicznych o łącznej długości około 3500 km (fig. 3–6). Do modelowania wykorzystano metodę inwersji tomograficznej. Zastosowany algorytm inwersji wykorzystuje czasy pierwszych wstąpień fal sejsmicznych. Jako dane wejściowe użyto około 2500 rejestracji sejsmicznych (fig. 3–5). Obszar objęty modelowaniem (fig. 1) jest prostopadłościanem o rozmiarach 816 km x 320 km i głębokości 64 km. Prędkość fal podłużnych jest zadana w sześciennych komórkach o rozmiarze 4 km. W wyniku przeprowadzonego modelowania otrzymano rozkład prędkości fal podłużnych w rejonie badań do głębokości około 40 km (fig. 7–12). Przy powierzchni modelu występują obszary o prędkości fal podłużnych < 6 km/s odpowiadające basenom osadowym na szelfie Półwyspu Antarktycznego. Grubość skorupy ziemskiej zmienia się od około 30 km pod Cieśniną Bransfielda do 35–40 km w południowej części obszaru badań. W centralnej części Cieśniny Bransfielda na głębokości około 10 km i więcej występują anomalnie wysokie prędkości fal podłużnych – powyżej 7,4 km/s, związane ze strukturą ryftową. Uzyskane wyniki wskazują, iż badany obszar można podzielić na część położoną na południe od strefy rozłamowej Hero, o typowo kontynentalnej budowie skorupy, i część północną, o anomalnie wysokich prędkościach fal podłużnych i cieńszej skorupie ziemskiej.